Tectonophysics 881 (2024) 230349

Contents lists available at ScienceDirect

Tectonophysics

journal homepage: www.elsevier.com/locate/tecto

Power law dependence of unstable slip velocity on decreasing shear loading stiffness

Lu Gu [a,b], Shengwang Hao [a,*], Derek Elsworth [c]

[a] School of Civil Engineering and Mechanics, Yanshan University, Qinhuangdao, China
[b] School of Resources and Civil Engineering, Liaoning Institute of Science and Technology, Benxi, China
[c] Energy and Mineral Engineering, Geosciences, G3 Center, and EMS Energy Institute, Pennsylvania State University, University Park, PA, USA

ARTICLE INFO

Keywords:
Shear loading stiffness
Peak slip velocity
Unstable slip
Power law
Slip acceleration

ABSTRACT

Shear loading stiffness plays a critical role in conditioning the stability of slip on reactivated faults. However, a relationship linking peak slip velocities and shear loading stiffness is lacking. To explore this, we shear granite faults in double direct shear with shear loading stiffnesses spanning two orders to define the effects of shear loading stiffness in conditioning the transition from stable to unstable slip. Our results show that peak slip velocity and acceleration decrease as power law relationships with respect to the shear loading stiffness ratio, with identical exponent, and with a linear relationship between the peak slip velocity and acceleration. The maximum acceleration occurs during the velocity weakening process that limits the peak slip velocity. The power law exponent increases linearly with increasing normal stress. Experimental results also indicate that slip magnitude, stress drop and recurrence time of unstable slip events increase, and slip durations decrease with decreasing stiffness ratios. The spans of limit cycles of velocity versus shear stress decrease, and their shapes evolve from triangular to semicircular with increasing loading stiffness ratio. Stress drops mostly occur during deceleration. The deceleration phase dominates the unstable slip duration that decreases as peak slip velocity increases. Our results indicate that the average stress drop rates over a slip duration increase as a power law relationship with reducing shear loading stiffness, which also contributes to a lower shear loading stiffness producing increased slip velocities and accelerations. Our findings highlight that loading stiffness ratio is an underlying mechanism defining unstable slip behaviors with the normal stress merely conditioning the exponent. The present relationship of unstable slip velocity with shear loading stiffness suggests a way to evaluate hazard of an impending instability event based on the initial shear loading stiffness ratio that can be calculated through the linear-elastic behaviors at the early quasi-static phase.

1. Introduction

Frictional slip on laboratory faults show a spectrum of responses that transit from slow to fast slip (Kaproth and Marone, 2013; Leeman et al., 2018) and mimic the response of natural faults. Slip velocities of natural faults range from several millimeters per year to tens of meters per second. After this instability transition of frictional slip, sliding accelerates unstably before finally decelerating to a new quasi-static state (Gu and Wong, 1991; Sone and Shimamoto, 2009; Im et al., 2017; Gu et al., 2023). Although some mechanisms, such as dilatant hardening (Segall et al., 2010; Samuelson et al., 2011) or a transition in frictional constitutive behavior with increasing slip velocity (Ghosh et al., 2012; Ikari et al., 2013; Kaproth and Marone, 2013; Im et al., 2020), are suggested to limit slip velocity, controls on the maximum slip velocity or acceleration in unstable sliding remain undefined.

Peak slip velocity and rupture speed are two physical parameters characterizing earthquakes and constraining kinematic model of faults. Faults can attain subshear through supershear propagation speeds (Xia et al., 2004, 2005; Schubnel et al., 2011; Tal et al., 2022). Laboratory experiments (Ohnaka, 1973; Ohnaka et al., 1987) and numerical results (Bizzarri, 2012) indicate the interdependence between the peak slip velocity and rupture speed. Peak slip velocity in unstable slip of faults is a fundamental dynamic parameter defining an earthquake, and is related to the magnitude of the event and the ground velocity (Bizzarri, 2012). Peak slip velocity and its timing provide clues to estimate the critical slip weakening distance and stress breakdown time (Mikumo

* Corresponding author.
E-mail address: hsw@ysu.edu.cn (S. Hao).

https://doi.org/10.1016/j.tecto.2024.230349
Received 17 February 2024; Received in revised form 14 April 2024; Accepted 10 May 2024
Available online 17 May 2024

et al., 2003; Tinti et al., 2004, 2009), although mechanisms that govern these are poorly constrained. Despite reports on the significance of peak slip velocity to ground motion prediction and hazard assessment (Bizzarri, 2012; Passelègue et al., 2016; Yao and Yang, 2023), the underlying processes defining the peak slip velocity remain elusive.

The criterion for slip instability depends on the ratio between the elastic stiffness of the loading system and the critical weakening rate (stiffness) of the fault (Ruina, 1983; Rice and Ruina, 1983; Gu et al., 1984). When the shear stress reaches the static frictional strength of the fault, slip initiates and the stored elastic energy surrounding the fault is released. Experimental and numerical results (Goodman and Sundaram, 1978; Gu and Wong, 1991; Kaproth and Marone, 2013; Leeman et al., 2015, 2016; Scuderi et al., 2017) indicate that the stiffness of the loading apparatus controls the development of unstable slip. Observations (Kaproth and Marone, 2013; Leeman et al., 2015, 2016) show that the full spectrum of fault slip behaviors, from slow to fast stick-slip, can be reproduced by varying the shear stiffness ratio of the loading frame to the fault with peak slip velocities changed from 50 to 100 μm per second to several millimeters per second. Although many studies indicate the dependence of peak slip velocities on the shear loading stiffness (Kaproth and Marone, 2013; Leeman et al., 2015; Tinti et al., 2016; Chen, 2023), no clear description of this relationship exist.

We develop a quantitative description linking the dependence of peak slip velocity and acceleration to this loading stiffness ratio based on systematic laboratory observations. Double direct shear tests are conducted with varying shear loading stiffnesses that span two orders of magnitude. Limitations on slip velocity are demonstrated by comparing evolutions of shear stresses against sliding velocities for different shear loading stiffnesses. From these observations, we quantify relationships between peak slip velocities and stress drop, slip duration and recurrence times.

2. Experimental materials and methods

Fault reactivation experiments are reported on granite interfaces in a servo-controlled double-direct shear apparatus at room temperature and humidity (Fig. 1). As shown in Fig. 1b, the simulated fault system comprises three precision-ground and polished blocks allowing a central forcing block to be sheared between two stationary side blocks. The dimensions of the side blocks are 40 mm × 36 mm × 40 mm with a central sliding block 40 mm × 36 mm × 80 mm. The nominal frictional contact area is 36 mm × 40 mm. X-ray diffraction (XRD) analysis shows that the granite sample comprises 46.5% diopside, 19.5% albite, 33.9% anorthite, and 0.2% quartz. The sample has a mean crystal size of ~680 μm (Hao et al., 2017). The uniaxial compressive strength is ~222 MPa, and the longitudinal P-wave velocity is ~6.7 km/s.

Normal stresses are applied horizontally by a gas compression actuator to the side blocks and shear stresses are applied vertically to the

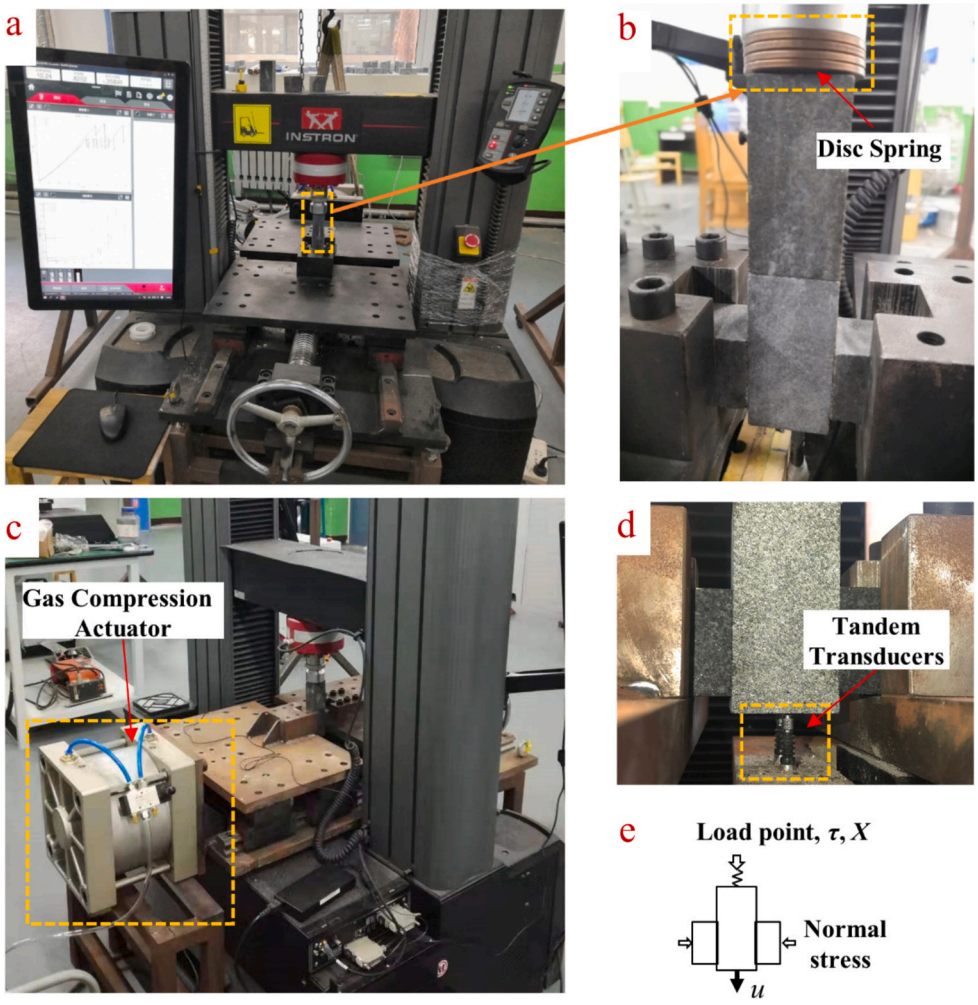

Fig. 1. Testing setup. (a) Double-direct shear test system. (b) Zoom-in on the sample and the disc springs. Disc spring (yellow dotted box in panel b) present between the moving platen and the sliding granite block. (c) Gas compression actuator (yellow dotted box) used to impose normal stresses. (d) Two tandem transducers (yellow dotted box) monitoring the slip displacement, u. (e) Schematic of double-direct shear configuration. (For interpretation of the references to colour in this figure legend, the reader is referred to the web version of this article.)

central blocks in an Instron 5982 testing machine. The current experiments simulate the condition where the energy release from the elastic environment surrounding the fault drives unstable slip. We posit that a decrease in normal stress reduces the critical stiffness of the fault and thus enhances stability (Im et al., 2017). Thus, initial stiffness ratio and normal stress are two key factors that determine the stability of slip. Our previous tests (Gu et al., 2023) demonstrate that for the loading stiffness of this system, a normal stress of 3.4 MPa produces significant stick-slip cycles. Prior experiments by others produce stick slip when normal stress is >1.5 MPa (Scholz et al., 1972) and also in the range 5–7 MPa (Im et al., 2017) and are even more common at higher normal stresses (Scholz et al., 1972; Tullis, 1996). Consequently, Reactivation experiments are performed at three normal stresses, σ_n = 3.4, 6.8 and 10.2 MPa with the central block driven at constant load point velocity, $V_L = 1$ mm/min. In the current experiments, the maximum normal stress of 10.2 MPa is a moderate stress for stick-slip experiments in the lab.

Shear force is monitored by an Instron 5982 Series load cell. This load cell comprises a full strain gauge bridge bonded to a stiff and linear elastic element. The load point displacement X is the crosshead displacement of the Instron testing machine that is measured by the Instron digital displacement sensor. This is a contacting transducer with low contact force and low friction to allow accurate measurement of linear displacement with respect to the reference surface. The sliding displacement, u, is recorded as the average of two tandem transducers (ZX–TDS04T high accuracy contact-type produced by OMRON Corporation) with a resolution of 0.1 μm that are attached under the central sliding block (Fig. 1). Shear force F, load point displacement X, and sliding displacement u are monitored and acquired at a sampling rate of 1000 Hz.

Shear loading stiffness is changed through a variable-height stack of disc springs (yellow dotted box in Fig. 1b) bridging the gap between the moving platen and the sliding granite block. We focus on the peak velocity of unstable slips with the stiffnesses of the loading system less than the critical stiffness required to produce regular stick-slip cycles.

3. Experimental results

3.1. Unstable slip behaviors defined by the shear loading stiffness

The shear loading stiffness is a key factor determining the sliding condition as either stable or unstable. Our previous experiments (Gu et al., 2023) illustrate that the present test system, with a stiffness of 127.1 kN/mm produces regular stick-slip cycles even under low normal stresses of 3.4 MPa. In order to investigate the relationship between peak

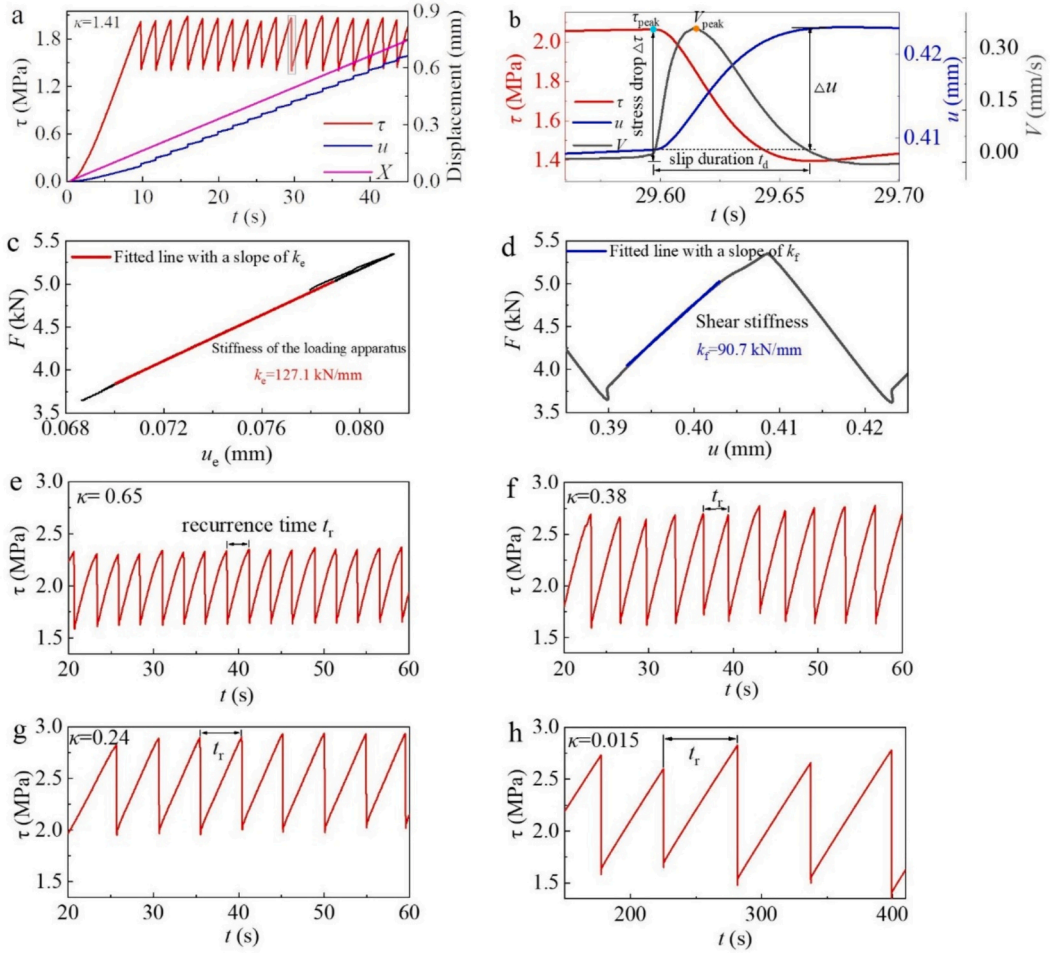

Fig. 2. Typical stick-slip results for five stiffness ratios. Slip duration t_d is the elapsed time between the maximum and minimum stresses within the stick-slip cycle. Δu is the sliding displacement increment between these two points. τ_{peak} is the peak shear stress, V_{peak} is the peak slip velocity in an individual stick-slip event. t_r is recurrence time, defined as the time interval between two successive stick-slip events. (a) Evolution of shear stress τ, load point displacement X, and sliding displacement u at a stiffness ratio $\kappa = 1.41$. (b) Zoom-in on a typical stick-slip event. Stress drop $\Delta\tau$ is defined as the difference between the maximum and minimum stress. (c) Determination of the stiffness of the loading apparatus, k_e. k_e is defined as the slope of the linear-elastic portion of shear force F versus the deformation of the loading apparatus u_e in a stick-slip event. (d) Determination of initial shear stiffness k_f of the frictional surfaces. k_f is defined as the slope of the linear-elastic portion of F-u in the loading process of an individual stick-slip event. (e-h) Stick-slip cycles for κ = 0.65, 0.38, 0.24, 0.015. κ is the stiffness ratio defined as the ratio of k_e to k_f.

unstable velocities and the loading stiffness, we perform experiments at this system stiffness and below to guarantee stick-slip events for all stiffnesses. Frictional sliding experiments are conducted under a broad range of shear loading stiffnesses ranging from 1.6 to 127.1 kN/mm, spanning two orders of magnitude. Fig. 2 shows plots of typical stick-slip cycles for different loading stiffness ratios. In these experiments, the slip durations of individual unstable slip events range from 0.053 s to 0.093 s. Thus, we use a high sampling rate of 1000 Hz to capture the rapid onset and short duration stick-slip events. Force versus sliding displacement of all stick-slip events in each experiment show similar evolution. Fig. 2 zooms-in on each experiment under different stiffnesses to illustrate the congruence of their evolution.

In order to clearly illustrate the effects of the shear loading stiffness on stick-slip behaviors, some fundamental physical quantities are defined as shown in Fig. 2. In an individual stick-slip event (Fig. 2b), the shear stress drop $\Delta\tau$ is the stress difference, the slip duration t_d is the time difference and Δu is the sliding displacement spanning the displacements at maximum and minimum shear stress. The shear loading stiffness of the apparatus k_e is defined as the slope of the linear-elastic portion of the curve of shear force (F) versus the deformation (u_e) of the loading apparatus (Fig. 2c), where $u_e = X\text{-}u$. The initial shear stiffness k_f of the frictional surfaces is measured as the slope of the linear-elastic portion of the F-u load curve (Fig. 2d). The stiffness ratio κ is defined as the ratio of k_e to k_f as.

$$\kappa = k_e/k_f. \tag{1}$$

Finally, recurrence time t_r is calculated as the time interval between two successive stick-slip events in the sequence (Figs. 2e-h).

Fig. 3 shows shear stress, sliding displacement, velocity and acceleration in each individual stick-slip event for different stiffness ratios. In the current experiments, stick-slip events are of slip durations 0.053 to 0.093 s and with average sliding displacements in individual cycles of 0.015 to 1.157 mm, and evolving from small to large events with decreasing stiffness ratios. Shear stress drops are 0.66 to 1.34 MPa and the recurrence time is 2 to 56.4 s in stick-slip events. Resolutions of 0.1 μm for slip displacement and 1 N (~6×10^{-4} MPa) for the loading are sufficient to record the evolution of the various stick-slip cycles. For all three normal stresses of σ_n = 3.4, 6.8 and 10.2 MPa, both shear stress drops and recurrence time increase with decreasing stiffness ratios (Figs. 2 and 3, Appendix Figs. 1 and 2).

3.2. Power law dependence of peak slip velocity and acceleration on shear loading stiffness

For different shear loading stiffnesses, each unstable slip event undergoes a similar sliding process from acceleration to deceleration (Fig. 3, Appendix Figs. 1 and 2). However, the peak slip velocity decreases from 3.43 to 0.38 mm/s and peak acceleration decreases from 508 to 40 mm/s^2 as the loading stiffness ratio is increased from 0.24 to 1.41. Thus, for a change in stiffness ratio spanning two orders, changes in peak slip velocity and acceleration span two orders in magnitude.

Fig. 4 shows how peak slip velocities (V_{peak}) and accelerations ($\dot{V}_{peak}$) respond to loading stiffness ratios at normal stresses of 3.4, 6.8 and 10.2 MPa. These experimental results indicate that both peak slip velocity and acceleration show power law dependences to loading stiffness ratios as.

$$\nu = C_v\kappa^{-\gamma v} \tag{2}$$

and

$$a = C_a\kappa^{-\gamma a}. \tag{3}$$

Where, $\nu = V_{peak}/V_L$ is the normalized peak slip velocity with V_L and a=$\dot{V}_{peak}$/g is the normalized peak slip acceleration with gravitational acceleration, g = 9.8 m/s^2. C_v and C_a are two constants. Interestingly, dependences of peak slip velocity and acceleration on the loading stiffness ratio share the same power law exponent for the same normal stress: $\gamma_v = \gamma_a$ = 0.93 for σ_n = 3.4 MPa, 1.18 for σ_n = 6.8 MPa, and 1.45 for σ_n = 10.2 MPa, respectively (Fig. 4). This is confirmed by the linear relationship of peak slip velocities and accelerations shown in Fig. 5. Values of exponents (γ_v and γ_a) increase linearly with normal stresses (Appendix Fig. 3).

3.3. Stress drop with velocity and acceleration

Fig. 6 illustrates the evolution of sliding velocities and accelerations with shear stresses under different shear loading stiffness ratios. The spans of limit cycles of velocity versus shear stress decrease, and their shapes evolve from triangular to semicircular with increasing stiffness ratio (Figs. 6a-c). These indicate that during each stick-slip cycle in unstable slip, the shear stress originally drops as convex upwards as slip velocity increases, before drops as convex-down as slip velocity decreases (Figs. 6a-c). Stress drops mostly occur during deceleration

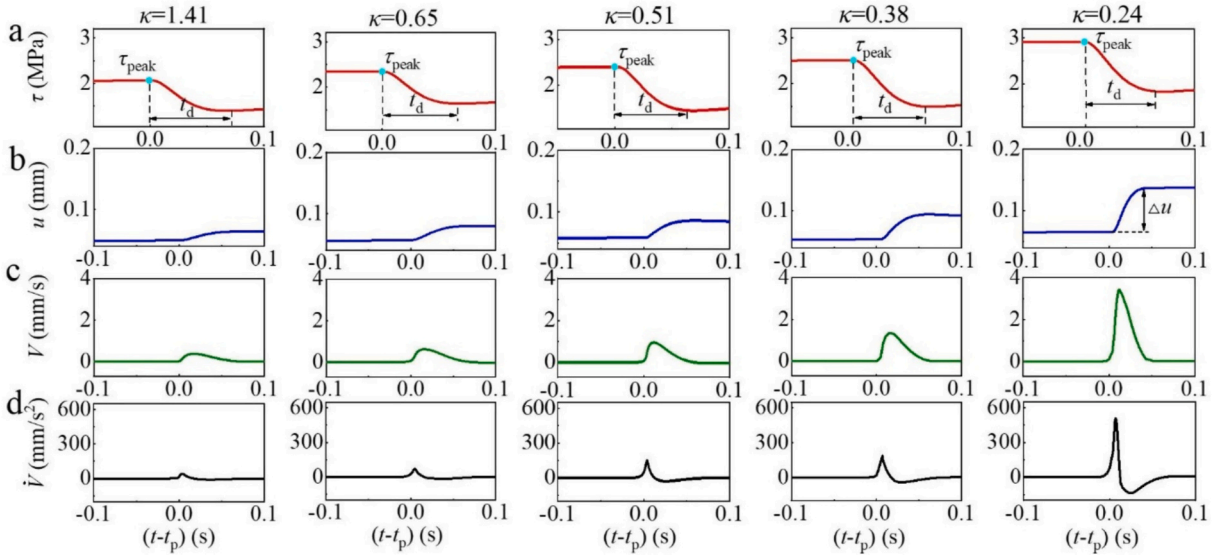

Fig. 3. Representative unstable slip events for five stiffness ratios when the normal stress is 3.4 MPa. (a) Shear stress τ. (b) Sliding displacement u. (c) Slip velocity V. (d) Slip acceleration $\dot{V}$. t_p is the time of peak shear stress in an individual stick-slip event.

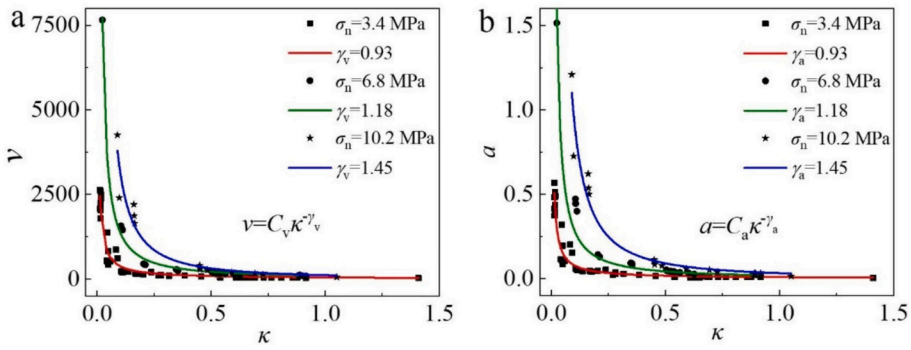

Fig. 4. Power law relationships between normalized peak (a) slip velocity and (b) acceleration with stiffness ratios under different normal stresses. Peak slip velocity and acceleration share the same exponent for the same normal stress. Values of exponents increase with normal stresses. Scattered experimental data (symbols) fitted by best-fit solid lines.

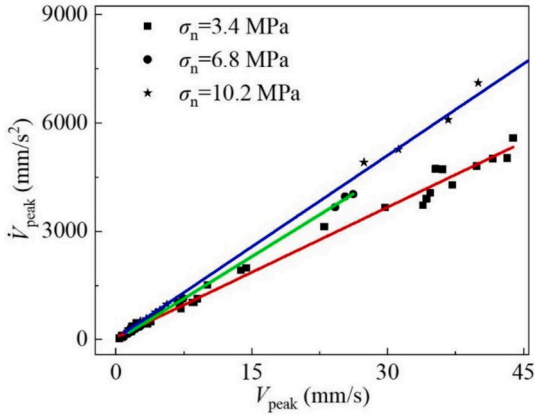

Fig. 5. Peak slip acceleration versus peak slip velocity. Scattered experimental data (symbols) fitted by best-fit solid lines.

(Figs. 6d-f).

3.4. Stick-slip period and unstable slip duration

With decreasing stiffness ratio, both stress drops and recurrence time increase, but slip duration decreases (Figs. 7a-c). Slip duration decreases as V_{peak} increases (Fig. 7d). The slip duration is much shorter than the recurrence time in each stick-slip event. Thus, differences in stick-slip periods under different stiffness ratios are dominated by differences in healing times.

4. Discussion

4.1. Energy release from the loading apparatus accelerates slip

Post-peak shear force, the shear loading apparatus releases its stored strain energy to accelerate the sliding. The sliding displacement, u, is the difference between the load point displacement (X) and the deformation (u_e) of the loading system as.

$$u = X - u_e. \tag{4}$$

Differentiating Eq. (4) with respect to time gives

$$V = V_L - V_e = V_L + \left(-\dot{F}\right)\Big/k_e. \tag{5}$$

Where, V_e is deformation release velocity, $\dot{F}$ is shear force rate as a proxy for stress drop rate. V_L is constant in the current experiments. Post-peak force, both V_e and $\dot{F}$ are negative since the stored strain energy is released from the loading apparatus. Eq. (5) indicates that reducing k_e results in a faster slip for the same stress drop. This is the underlying mechanism that results in a higher slip velocity (or acceleration) for a lower shear loading stiffness. Fig. 8 illustrates evolutions of average stress drop rates ($\Delta\tau/t_d$) and average slip velocities ($\Delta u/t_d$) versus loading stiffness ratios when the normal stress is 3.4 MPa. The ratio $\Delta\tau/t_d$ increases faster when loading stiffness ratio is reduced (Fig. 8a)

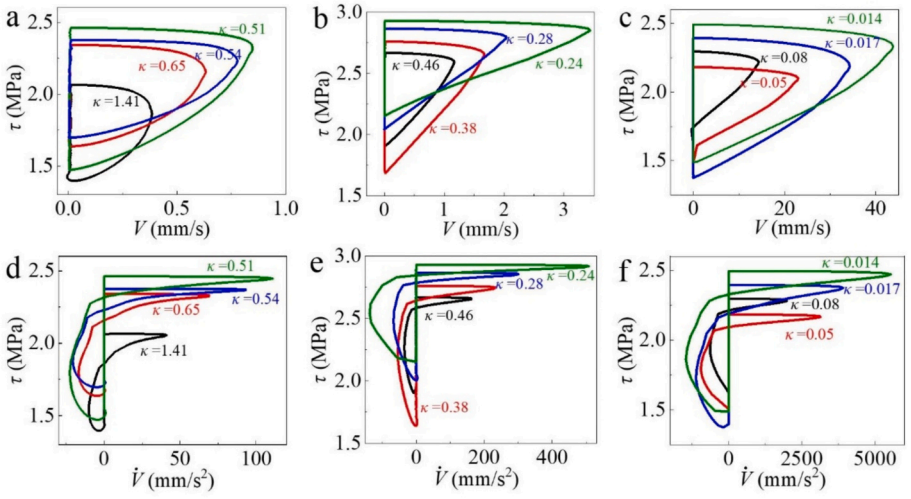

Fig. 6. Phase diagram showing shear stress evolution against sliding (a-c) velocity and (d-f) acceleration during stick-slip cycles under different stiffness ratios.

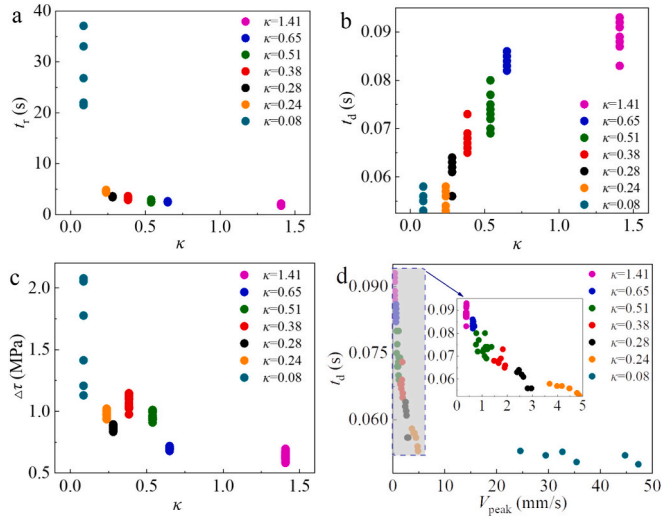

Fig. 7. Parameters defining unstable slips. (a) Recurrence time, (b) slip duration and (c) stress drop as a function of stiffness ratios. (d) Plots of slip duration as a function of peak slip velocity. The inset shows a zoom-in of the shaded area.

also contributing to a lower shear loading stiffness producing increased slip velocities and accelerations. Both normalized average stress drop rates $((\Delta\tau/t_d)/(\Delta\tau/t_d)_{max})$ and average slip velocities $((\Delta u/t_d)/V_L)$ decrease as a power law relationship with the shear loading stiffness ratio (Fig. 8).

4.2. End-member response at high and low shear loading stiffness ratios

We observe an empirical relationship between unstable slip velocity and shear loading stiffness ratio. Our stiffness ratios cover a limit range. However, it is evident that when the stiffness ratio is very large, so that no unstable slip occurs, then the slider will move at the load point velocity. Thus, the unstable slip velocity is zero. Our experiments are restricted to the unstable slip regime – thus, the slip velocity during unstable slip phase is much greater than prescribed load point velocity. The power law relationship of Eq. (2) describes the dependence of unstable slip velocity on the loading stiffness ratio, which is insensitive to load point velocity. Prediction of the relationship of Eq. (2) also accommodates the case where the unstable slip velocity is zero when the stiffness ratio is very large.

The current experimental results do not probe the velocity response for very low stiffness ratios – as these were unreachable in our current experimental configuration. However, these much approach the load point velocity, in the limit, as a consequence of stable sliding. Also, when the stiffness ratio is very low, the unstable slip velocity or acceleration cannot tend to infinity as predicted by Eqs. (2) and (3) when the stiffness tends to zero –as this is limited by the inertial response. The slip velocity should tend to a limiting value under very low stiffness ratios.

4.3. Linear relationship between peak slip velocities and accelerations

Our results show that parameters characterizing earthquake magnitude, such as stress drop, slip displacement, slip duration and stick-slip recurrence time are directly related to peak slip velocity. Our findings, that peak slip velocities have a linear relationship with peak accelerations, suggest the limitation of peak acceleration is a mechanism that limits the unstable slip velocity and the magnitude of earthquake events. Acceleration is defined by the inertial force that is also conditioned by an effective mass (of the slider). By definition, the inertial force is the difference between the applied shear and reactive frictional forces. Evolutions of slip accelerations (Figs. 6d-f) imply that the inertial force undergoes an evolution from first increasing to then decreasing during the unstable slip cycle. Some mechanisms have been proposed to explain this limitation on slip velocity (Segall et al., 2010; Kaproth and Marone, 2013; Ikari et al., 2013; Im et al., 2020). Our results show that the maximum acceleration occurs during the velocity weakening process (Fig. 6) that limits the peak slip velocity. The slip acceleration is determined by interactions between the decreasing shear force and frictional weakening. Our findings suggest that the maximum difference between shear and frictional forces in unstable slip determines the peak slip velocity. This is a fundamental cause limiting slip velocity.

4.4. Implications of experiments results

Our experiments explore the dependence of parameters characterizing the occurrence of slip instability events. These include the influence of magnitude, slip duration, recurrence time, stress drop, average stress rate, peak velocity and peak acceleration as conditioned by the shear loading stiffness. These systematic and constrained experiments illuminate the mechanisms responsible for unstable slip. The observed events span a wide range of fault stiffnesses and thus are applicable to a wide variety of natural fault conditions.

The current experiments show that shear loading stiffness exerts an essential control on the velocity of the unstable slips and on the stress drop magnitude of these events. The influence of the shear loading stiffness on peak slip velocity has been previously observed (Kaproth and Marone, 2013; Leeman et al., 2015, 2016). However, we provide a description of the dependence of peak slip velocity on the shear loading stiffness and thus further define the actual relationship. These findings thus illuminate the mechanisms controlling the slip velocity and stress drop magnitude of the unstable events. In this study, peak slip velocities range from 0.38 to 43.85 mm/s, spanning two orders of magnitude. The experimental results are consistent with stick-slip velocities inferred for regular, fast earthquakes (Tinti et al., 2016; Mai and Thingbaijam,

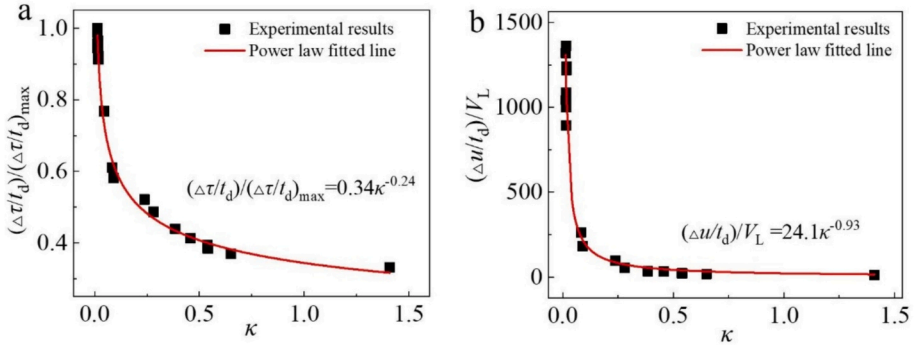

Fig. 8. Power law relationships of (a) normalized average stress drop rates $(\Delta\tau/t_d)/(\Delta\tau/t_d)_{max}$, and (b) normalized average slip velocities $(\Delta u/t_d)/V_L$ with stiffness ratios when the normal stress is 3.4 MPa.

2014). This means that the key processes that generate stick-slip in laboratory experiments may be operational in natural faults. Thus, these results provide insight in understanding and interpreting why natural earthquakes occur with a broad spectrum of slip velocities and show different stress drop magnitudes, which remain enigmatic.

We define a relationship linking peak slip velocity and shear loading stiffness. This may serve as a guidance in designing experiments, numerical simulations and model development to explore the nature of unstable slip. Theoretical and experimental results (Kaproth and Marone, 2013; Leeman et al., 2015, 2016; Kilgore et al., 2017) show the coupled effects of the shear loading stiffness and normal stress in defining the sliding behavior. Our results define the different effects of normal stress and the shear loading stiffness on unstable slip.

5. Conclusions

Experiments of unstable slip on laboratory faults exhibit a significant dependence on the shear loading stiffness. With decreasing stiffness ratios, all of slip magnitude, stress drop and recurrence time of unstable slip events increase, but slip duration decreases. Slip durations show smaller differences than recurrence time and are much shorter than static-stick duration, and thus static-stick duration dominates the recurrence time. Average stress drop rates and average slip velocities increase with decreased shear loading stiffness. Notably, peak slip velocity and acceleration increase with decreased loading stiffness ratio as a power law relationship. The power law exponent is identical for both peak slip velocities and accelerations, but increases linearly with increased normal stress. Peak slip velocities are linearly related to peak accelerations. The maximum acceleration occurs during the velocity weakening process.

Each unstable slip event undergoes a similar sliding process from acceleration to deceleration, and its duration is dominated by the deceleration phase. The spans of limit cycles of velocity versus shear stress decrease, and their shapes evolve from triangular to semicircular with increasing loading stiffness ratio. Phase diagrams of shear stress evolution against sliding acceleration in stick-slip cycles show that stress drops mostly occur in the deceleration process. A general energy analysis indicates that reducing shear loading stiffness results in a faster slip – for the same stress drop, which is the underlying mechanism that results in a higher slip velocity (or acceleration) for a lower shear loading stiffness. The average stress drop rates over a slip duration increase as a power law relationship with reducing shear loading stiffness, which also contributes to a lower shear loading stiffness producing increased slip velocities and accelerations.

CRediT authorship contribution statement

Lu Gu: Writing – original draft, Methodology, Investigation, Formal analysis, Data curation. **Shengwang Hao:** Writing – review & editing, Supervision, Resources, Project administration, Funding acquisition. **Derek Elsworth:** Writing – review & editing, Supervision.

Declaration of competing interest

The authors declare that they have no known competing financial interests or personal relationships that could have appeared to influence the work reported in this paper.

Data availability

Data will be made available on request.

Acknowledgments

This work is supported by Hebei Natural Science Foundation (Grant No. D2020203001), Key Research and Development Projects of Hebei Province (Grant No. 22375407D), National Natural Science Foundation of China (Grant No. 11672258) and Foundation of Education Department of Liaoning Province (Grant No. LJKZ1075, LJKQZ20222473). DE gratefully acknowledges support from the G. Albert Shoemaker endowment.

Appendix A. Unstable slip results of variable shear loading stiffness when normal stresses were 6.8 and 10.2 MPa, and the relationship of power law exponents versus normal stresses

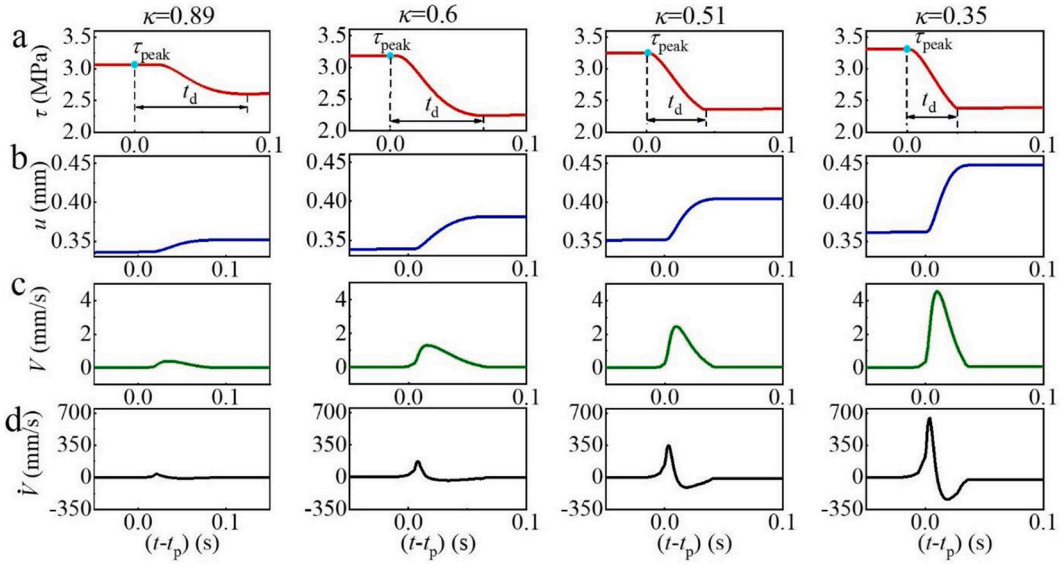

Appendix Fig. 1. Representative unstable slip events for four stiffness ratios when the normal stress was 6.8 MPa. (a) Shear stress τ. (b) Sliding displacement u. (c) Slip velocity V. (d) Slip acceleration $\dot{V}$. t_p is the time of peak shear stress in an individual stick-slip event

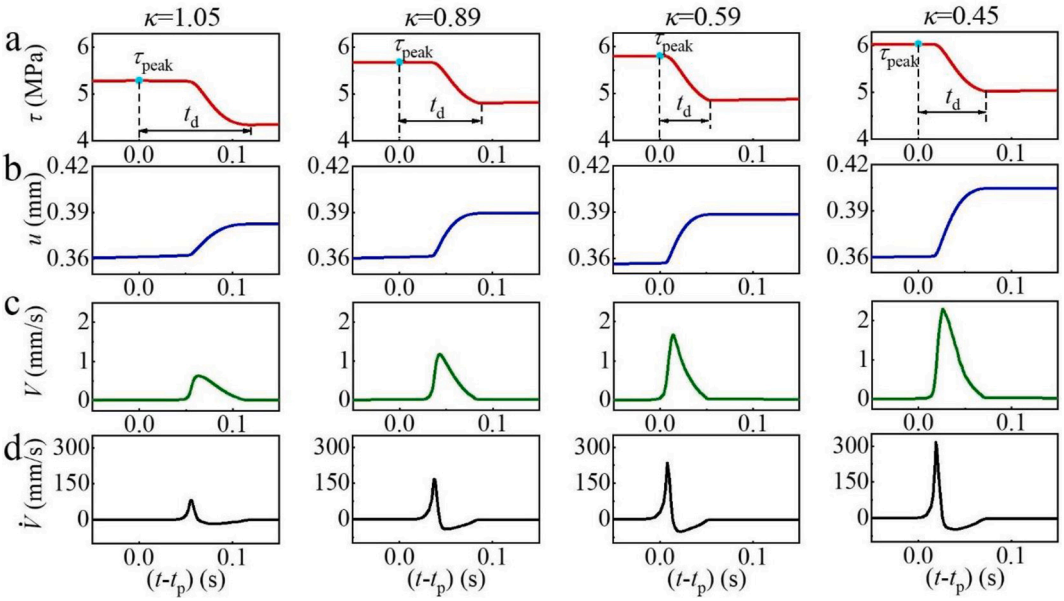

Appendix Fig. 2. Representative unstable slip events for four stiffness ratios when the normal stress was 10.2 MPa. (a) Shear stress τ. (b) Sliding displacement u. (c) Slip velocity V. (d) Slip acceleration $\dot{V}$. t_p is the time of peak shear stress in an individual stick-slip event

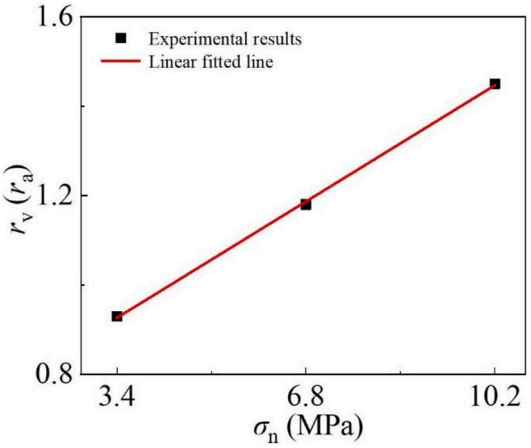

Appendix Fig. 3. Linear relationship between power law exponents and normal stresses.

References

Bizzarri, A., 2012. Rupture speed and slip velocity: What can we learn from simulated earthquakes? Earth Planet. Sci. Lett. 317, 196–203. https://doi.org/10.1016/j.epsl.2011.11.023.

Chen, J.Y., 2023. The emergence of four types of slow slip cycles on dilatant, fluid saturated faults. J. Geophys. Res. Solid Earth 128 (2), e2022JB024382. https://doi.org/10.1029/2022jb024382.

Ghosh, A., Vidale, J.E., Creager, K.C., 2012. Tremor asperities in the transition zone control evolution of slow earthquakes. J. Geophys. Res. Solid Earth 117 (B10). https://doi.org/10.1029/2012jb009249.

Goodman, R.E., Sundaram, P.N., 1978. Fault and system stiffnesses and stick-slip phenomena. Pure Appl. Geophys. 116, 873–887. https://doi.org/10.1007/bf00876543.

Gu, Y.J., Wong, T.-F., 1991. Effects of loading velocity, stiffness, and inertia on the dynamics of a single degree of freedom spring-slider system. J. Geophys. Res. Solid Earth 96 (B13), 21677–21691. https://doi.org/10.1029/91jb02271.

Gu, J.C., Rice, J.R., Ruina, A.L., et al., 1984. Slip motion and stability of a single degree of freedom elastic system with rate and state dependent friction. J. Mech. Phys. Solids 32 (3), 167–196. https://doi.org/10.1016/0022-5096(84)90007-3.

Gu, L., Hao, S.W., Elsworth, D., 2023. Precursory predictors of the onset of stick-slip frictional instability. Int. J. Solids Struct. 264, 112119 https://doi.org/10.1016/j.ijsolstr.2023.112119.

Hao, S.W., Yang, H., Elsworth, D., 2017. An accelerating precursor to predict "time-to-failure" in creep and volcanic eruptions. J. Volcanol. Geotherm. Res. 343, 252–262. https://doi.org/10.1016/j.jvolgeores.2017.07.009.

Ikari, M.J., Marone, C., Saffer, D.M., et al., 2013. Slip weakening as a mechanism for slow earthquakes. Nat. Geosci. 6 (6), 468–472. https://doi.org/10.1038/ngeo1818.

Im, K., Elsworth, D., Marone, C., et al., 2017. The impact of frictional healing on stick-slip recurrence interval and stress drop: Implications for earthquake scaling. J. Geophys. Res. Solid Earth 122 (12), 10102–10117. https://doi.org/10.1002/2017jb014476.

Im, K., Saffer, D.M., Marone, C., et al., 2020. Slip-rate-dependent friction as a universal mechanism for slow slip events. Nat. Geosci. 13 (10), 705–710. https://doi.org/10.1038/s41561-020-0627-9.

Kaproth, B.M., Marone, C., 2013. Slow earthquakes, preseismic velocity changes, and the origin of slow frictional stick-slip. Science 341 (6151), 1229–1232. https://doi.org/10.1126/science.1239577.

Kilgore, B.N., Beeler, M., Lozos, J., et al., 2017. Rock friction under variable normal stress. J. Geophys. Res. Solid Earth 122, 7042–7075. https://doi.org/10.1002/2017jb014049.

Leeman, J.R., Scuderi, M.M., Marone, C., et al., 2015. Stiffness evolution of granular layers and the origin of repetitive, slow, stick-slip frictional sliding. Granul. Matter 17, 447–457. https://doi.org/10.1007/s10035-015-0565-1.

Leeman, J.R., Saffer, D.M., Scuderi, M.M., et al., 2016. Laboratory observations of slow earthquakes and the spectrum of tectonic fault slip modes. Nat. Commun. 7 (1), 11104. https://doi.org/10.1038/ncomms11104.

Leeman, J.R., Marone, C., Saffer, D.M., 2018. Frictional mechanics of slow earthquakes. J. Geophys. Res. Solid Earth 123 (9), 7931–7949. https://doi.org/10.1029/2018jb015768.

Mai, P.M., Thingbaijam, K.K.S., 2014. SRCMOD: An online database of finite-fault rupture models. Seismol. Res. Lett. 85 (6), 1348–1357. https://doi.org/10.1785/0220140077.

Mikumo, T., Olsen, K.B., Fukuyama, E., et al., 2003. Stress-breakdown time and slip-weakening distance inferred from slip-velocity functions on earthquake faults. Bull. Seismol. Soc. Am. 93 (1), 264–282. https://doi.org/10.1785/0120020082.

Ohnaka, M., 1973. Experimental studies of stick-slip and their application to the earthquake source mechanism. J. Phys. Earth 21 (3), 285–303. https://doi.org/10.4294/jpe1952.21.285.

Ohnaka, M., Kuwahara, Y., Yamamoto, K., 1987. Constitutive relations between dynamic physical parameters near a tip of the propagating slip zone during stick-slip shear failure. Tectonophysics 144 (1-3), 109–125. https://doi.org/10.1016/0040-1951(87)90011-4.

Passelègue, F.X., Schubnel, A., Nielsen, S., et al., 2016. Dynamic rupture processes inferred from laboratory microearthquakes. J. Geophys. Res. Solid Earth 121 (6), 4343–4365. https://doi.org/10.1002/2015jb012694.

Rice, J.R., Ruina, A.L., 1983. Stability of steady frictional slipping. J. Appl. Mech. 50 (2), 343–349. https://doi.org/10.1115/1.3167042.

Ruina, A.L., 1983. Slip instability and state variable friction laws. J. Geophys. Res. Solid Earth 88 (B12), 10359–10370. https://doi.org/10.1029/JB088iB12p10359.

Samuelson, J., Elsworth, D., Marone, C., 2011. Influence of dilatancy on the frictional constitutive behavior of a saturated fault zone under a variety of drainage conditions. J. Geophys. Res. Solid Earth 116 (B10). https://doi.org/10.1029/2011jb008556.

Scholz, C., Molnar, P., Johnson., T., 1972. Detailed studies of frictional sliding of granite and implications for the earthquake mechanism. J. Geophys. Res. 77 (32), 6392–6406. https://doi.org/10.1029/jb077i032p06392.

Schubnel, A., Nielsen, S., Taddeucci, J., et al., 2011. Photo-acoustic study of subshear and supershear ruptures in the laboratory. Earth Planet. Sci. Lett. 308 (3-4), 424–432. https://doi.org/10.1016/j.epsl.2011.06.013.

Scuderi, M.M., Collettini, C., Viti, C., et al., 2017. Evolution of shear fabric in granular fault gouge from stable sliding to stick slip and implications for fault slip mode. Geology 45 (8), 731–734. https://doi.org/10.1130/g39033.1.

Segall, P., Rubin, A.M., Bradley, A.M., et al., 2010. Dilatant strengthening as a mechanism for slow slip events. J. Geophys. Res. Solid Earth 115 (B12). https://doi.org/10.1029/2010jb007449.

Sone, H., Shimamoto, T., 2009. Frictional resistance of faults during accelerating and decelerating earthquake slip. Nat. Geosci. 2 (10), 705–708. https://doi.org/10.1038/ngeo637.

Tal, Y., Rubino, V., Rosakis, A.J., et al., 2022. Dynamics and near-field surface motions of transitioned supershear laboratory earthquakes in thrust faults. J. Geophys. Res. Solid Earth 127 (3), e2021JB023733. https://doi.org/10.1029/2021jb023733.

Tinti, E., Bizzarri, A., Piatanesi, A., et al., 2004. Estimates of slip weakening distance for different dynamic rupture models. Geophys. Res. Lett. 31 (2) https://doi.org/10.1029/2003gl018811.

Tinti, E., Cocco, M., Fukuyama, E., et al., 2009. Dependence of slip weakening distance (D_c) on final slip during dynamic rupture of earthquakes. Geophys. J. Int. 177 (3), 1205–1220. https://doi.org/10.1111/j.1365-246x.2009.04143.x.

Tinti, E., Scuderi, M., Scognamiglio, L., et al., 2016. On the evolution of elastic properties during laboratory stick-slip experiments spanning the transition from slow slip to dynamic rupture. J. Geophys. Res. Solid Earth 121 (12), 8569–8594. https://doi.org/10.1002/2016jb013545.

Tullis, T.E., 1996. Rock friction and its implications for earthquake prediction examined via models of Parkfield earthquakes. Proc. Natl. Acad. Sci. USA 93 (9), 3803–3810. https://doi.org/10.1073/pnas.93.9.3803.

Xia, K.W., Rosakis, A.J., Kanamori, H., 2004. Laboratory earthquakes: the sub-Rayleigh-to-supershear rupture transition. Science 303 (5665), 1859–1861. https://doi.org/10.1126/science.1094022.

Xia, K.W., Rosakis, A.J., Kanamori, H., 2005. Supershear and subrayleigh to supershear transition observed in laboratory earthquake experiments. Exp. Tech. 29, 63–66. https://doi.org/10.1111/j.1747-1567.2005.tb00220.x.

Yao, S.L., Yang, H.F., 2023. Towards ground motion prediction for potential large earthquakes from interseismic locking models. Earth Planet. Sci. Lett. 601, 117905 https://doi.org/10.1016/j.epsl.2022.117905.